SUPPLEMENTARY INFORMATION

Hippocampal CA1 pyramidal cells form functionally distinct sublayers

Kenji Mizuseki, Kamran Diba, Eva Pastalkova and György Buzsáki

SUPPLEMENTARY METHODS

Detection of phasic REM

REM epochs were detected as described in Online Methods. Phasic REM epochs were detected as following. First, LFP trace during REM epochs were band-pass filtered (5-12 Hz), yielding y(t). Amplitude of theta oscillations were derived from Hilbert transform of y(t), and peaks of theta oscillations were detected as the positive to negative zero crossings of the derivative dy/dt. Inter-peak intervals were smoothed using an eleven-sample rectangular kernel. Candidate epochs were detected if smoothed inter-peak intervals were shorter than 10 percentile of smoothed inter-peak intervals. The candidate epochs were identified as phasic REM epochs if the following criteria were all fulfilled. (1) Duration of an epoch was longer than 900 msec. (2) Minimum of smoothed inter-peak intervals during an epoch was shorter than 5 percentile of smoothed inter-spike intervals. (3) Mean amplitude of theta oscillations during an epoch was larger than mean amplitude of theta oscillations during the entire REM sleep. A total of 5844 sec (3.68 % of REM sleep episodes) was identified as phasic REM epochs.

Firing rate correlations between left and right journeys on the linear track

First, smoothed firing rate maps were constructed as described in Online Methods. Firing rate correlations (Pearson product moment correlation coefficient) between left vs right journeys on the linear track were computed in two different ways. First, bin-by-bin firing rate correlation between the left and right journeys was calculated (**Supplementary Fig. 10i**). This correlation provides information about the strength of rate-position relationship of a neuron, when position is referenced to distant (room) cues. Second, the firing rate map during left journeys was reversed, and bin-by-bin firing rate correlation between the right journeys and reversed left journeys was calculated (**Supplementary Fig. 10j**). This correlation provides information about the strength of rate-position relationship of a neuron, when position is referenced to the start (or goal) position[1].

SUPPLEMENTARY REFERENCES

1. Gothard KM, Skaggs WE, Moore KM, McNaughton BL. Binding of hippocampal CA1 neural activity to multiple reference frames in a landmark-based navigation task. *J Neurosci*. **16**, 823–35 (1996).
2. Mizuseki,K., Sirota,A., Pastalkova,E., & Buzsaki,G. Theta oscillations provide temporal windows for local circuit computation in the entorhinal-hippocampal loop. *Neuron* **64**, 267–280 (2009).

Figure S1

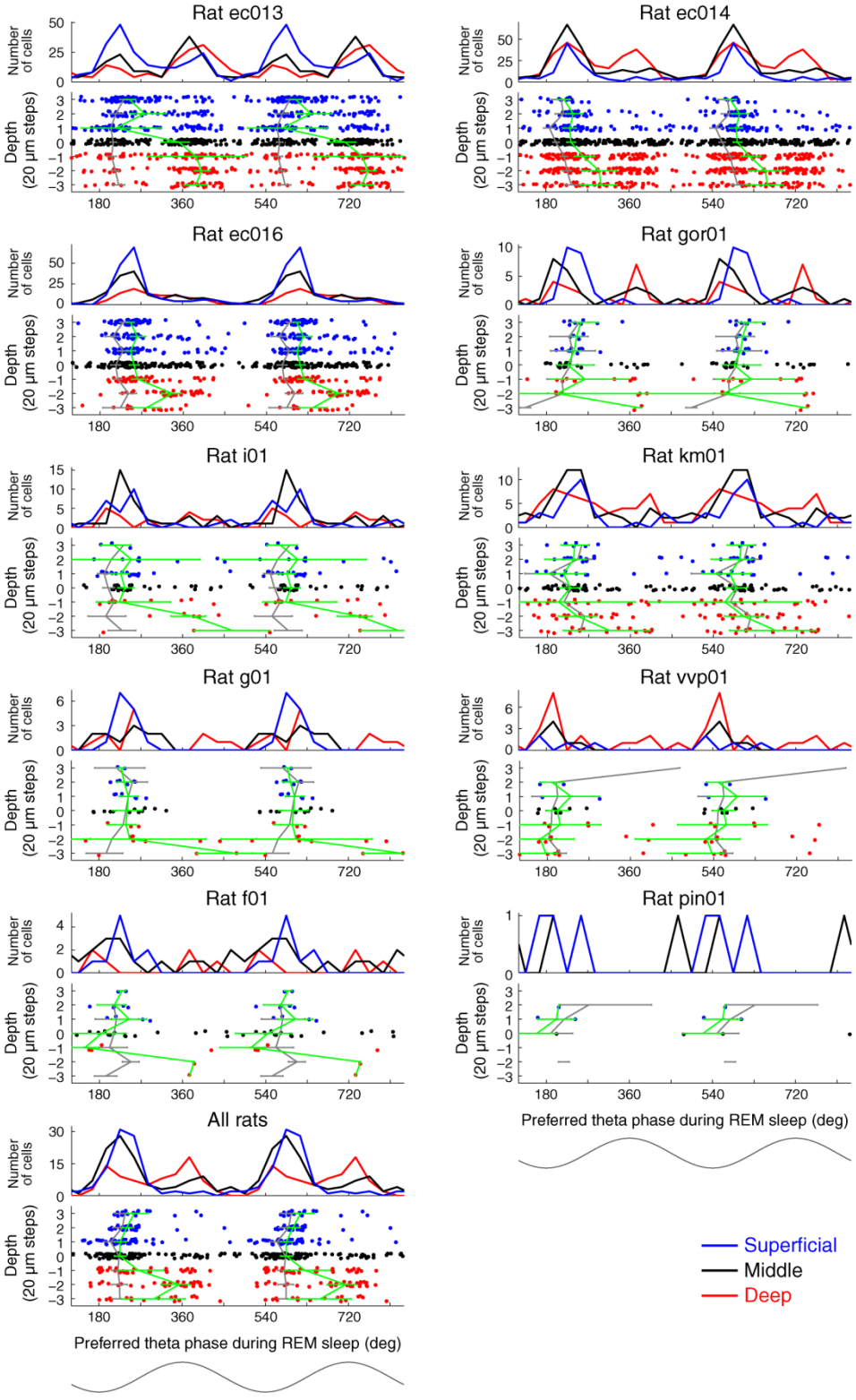
Rat ec013
Rat ec014
Rat ec016
Rat gor01
Rat i01
Rat km01
Rat g01
Rat vvp01
Rat f01
Rat pin01
All rats
Number of cells
Depth (20 µm steps)
Preferred theta phase during REM sleep (deg)
Superficial
Middle
Deep

Supplementary Fig. 1. Preferred theta phase of spikes during REM sleep depends on the position of the cell body within the CA1 pyramidal layer (data for individual rats). Top, distribution of the preferred theta phase of pyramidal cells in the superficial (blue), middle (black) and deep (red) sublayers during REM sleep. Bottom, position of cell and preferred theta phase during REM, each dot represents a single neuron. The few neurons above and below recording sites 3 and –3 were added to values at 3 and –3, respectively. Position 0, approximate middle of the layer (black dots) was determined by the maximum of ripple power for each shank in each session (see **Fig. 1**). Green and gray color lines, mean (± 95% confidence intervals) of preferred theta phase of pyramidal cells during REM and RUN at different depths of the layer, respectively. Each panel is from a different rat. Note the deeper position of REM-shifting neurons. All rats panel: group average of depth-dependent theta phase preference calculated from a single session in each rat.

Figure S2

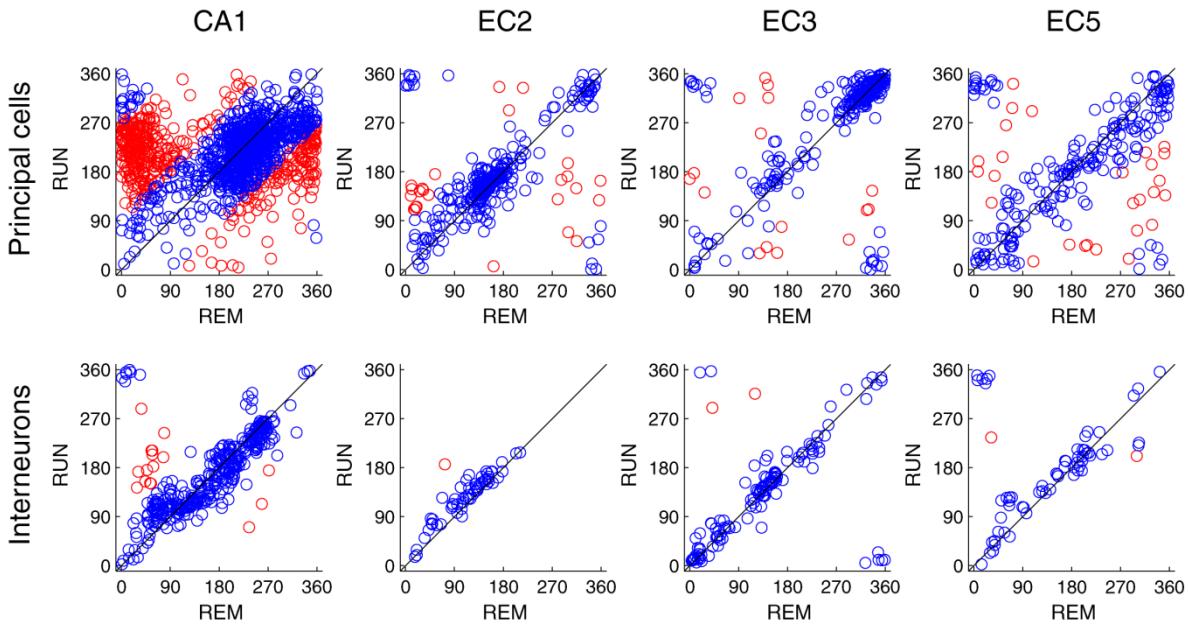

Supplementary Fig. 2. State-dependent shifting of theta phase preference is most prominent in the CA1 region. Distribution of preferred theta phases during RUN and REM sleep. Only neurons which showed significant theta phase modulation during both RUN and REM sleep are included (CA1 principal cells are the same as in **Fig. 2**). Only a small fraction of principal cells in the entorhinal cortex (EC2, EC3, EC5, layers II, III and V, respectively) showed REM-related > 90^{o} theta phase shift (red circles). Interneurons in all regions preferred the same theta phase across states. CA1 cells were referenced to theta oscillations recorded from CA1 pyramidal layer. EC cells were referenced to theta recorded from EC layer III.

Figure S3

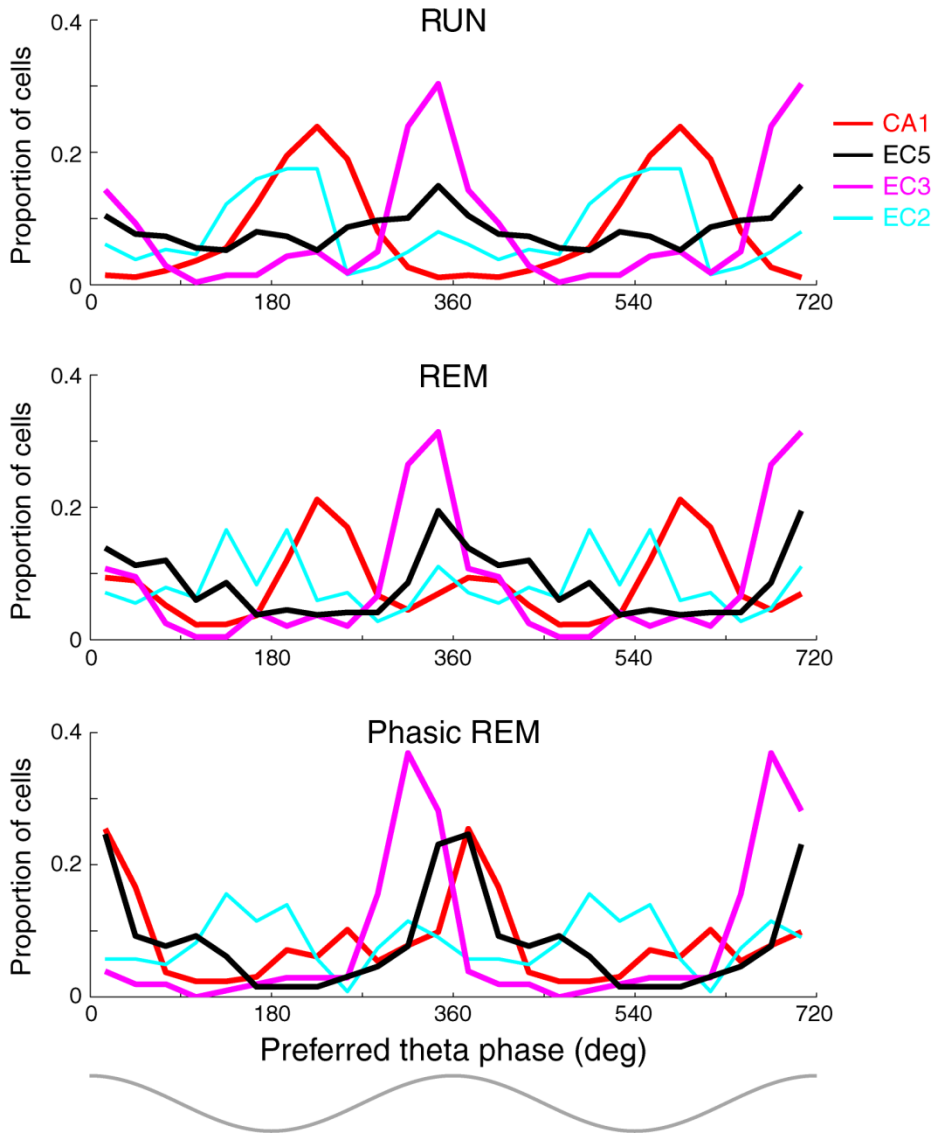

Supplementary Fig. 3. State-dependent theta phase preference of spikes in the CA1 region and entorhinal cortex. Preferred theta phase of CA1, entorhinal layer 2 (EC2), layer 3 (EC3) and layer 5 (EC5) principal neurons during RUN, REM and phasic REM sleep. Note the phase stability of entorhinal neurons across brain states. Note that while the majority of CA1 pyramidal cells fired at the trough of theta during RUN, the majority of CA1 neurons fired at the peak of theta during phasic REM sleep, approximately 60^{o} after the EC3 neurons. All cells were referenced to theta oscillations recorded from CA1 pyramidal layers. Bottom gray trace, idealized reference theta cycle in CA1 pyramidal layer.

Figure S4

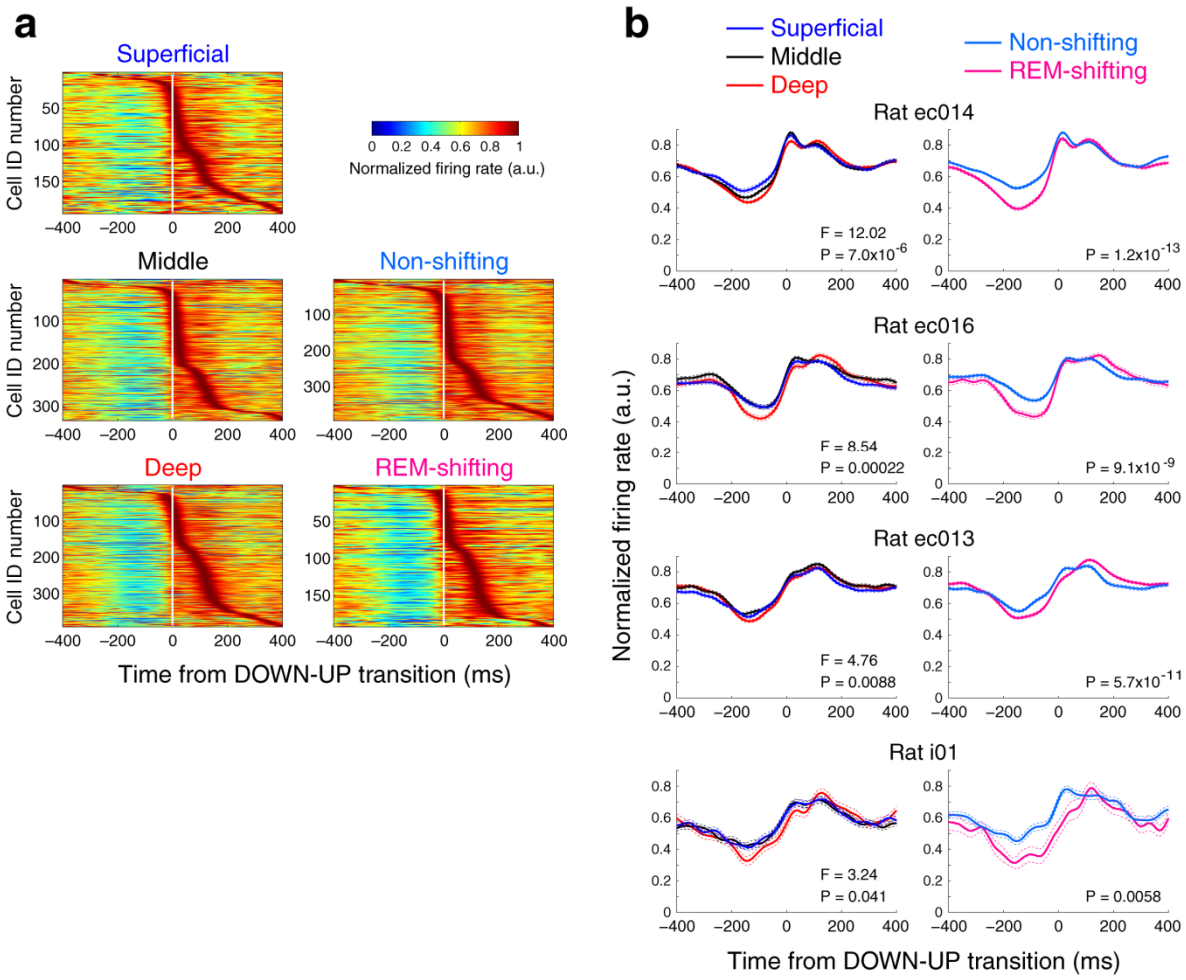

Supplementary Fig. 4. Phase-locking magnitude of CA1 pyramidal cell spikes by slow oscillations is location-dependent. a, Normalized, color-coded peri-event firing rate histograms of CA1 pyramidal neurons in deep, middle and superficial sublayers during SWS in the presence of slow oscillations (left). Time zero: DOWN-UP transition of slow oscillation, determined by the population activity of entorhinal cortex neurons (**Fig. 3**, see Online Methods). Each row is a single neuron recorded from rat ec014 equipped with electrodes in both hippocampus and entorhinal cortex. Right, normalized rate histograms of REM-shifting and non-shifting neurons. **b,** Left panels, normalized rate histograms of CA1 pyramidal neurons in the deep, middle and superficial sublayers during slow oscillations in sleep, shown separately in each rat. Means ± S.E.M. are shown. Right panels, normalized rate histograms of REM-shifting and non-shifting neurons in each rat. Significance levels are indicated in each panel.

Figure S5

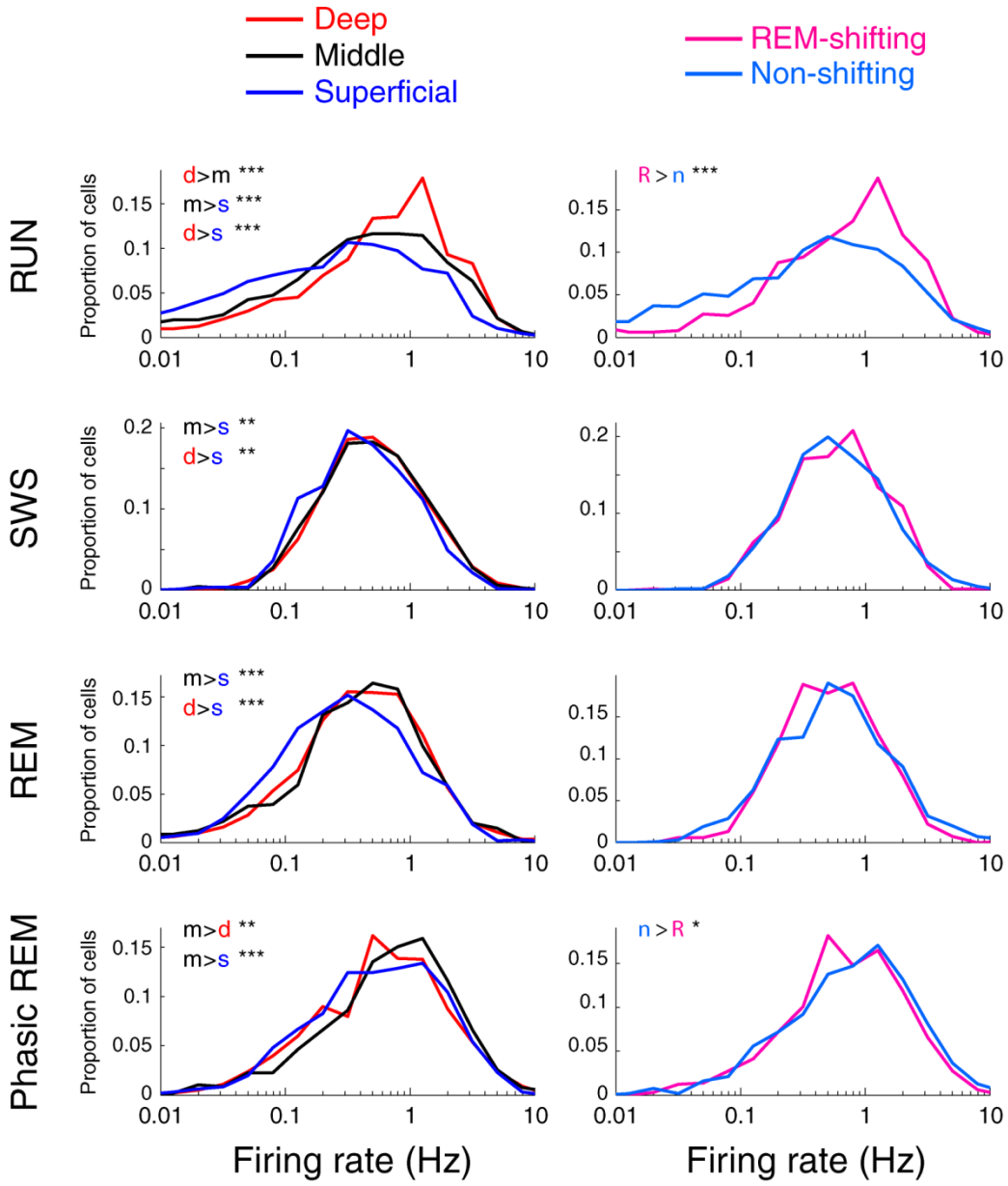

Supplementary Fig. 5. Firing rates of CA1 pyramidal neurons depend on both the network state and the somatic location within the CA1 pyramidal layer. Distribution of firing rates in different states, shown separately for deep, middle and superficial group (left) or REM-shifting and non-shifting neurons (right). ***, P<0.0001, **,P<0.001, *,P<0.01, two-sample Kolmogorov-Smirnov test, one-tailed.

Figure S6

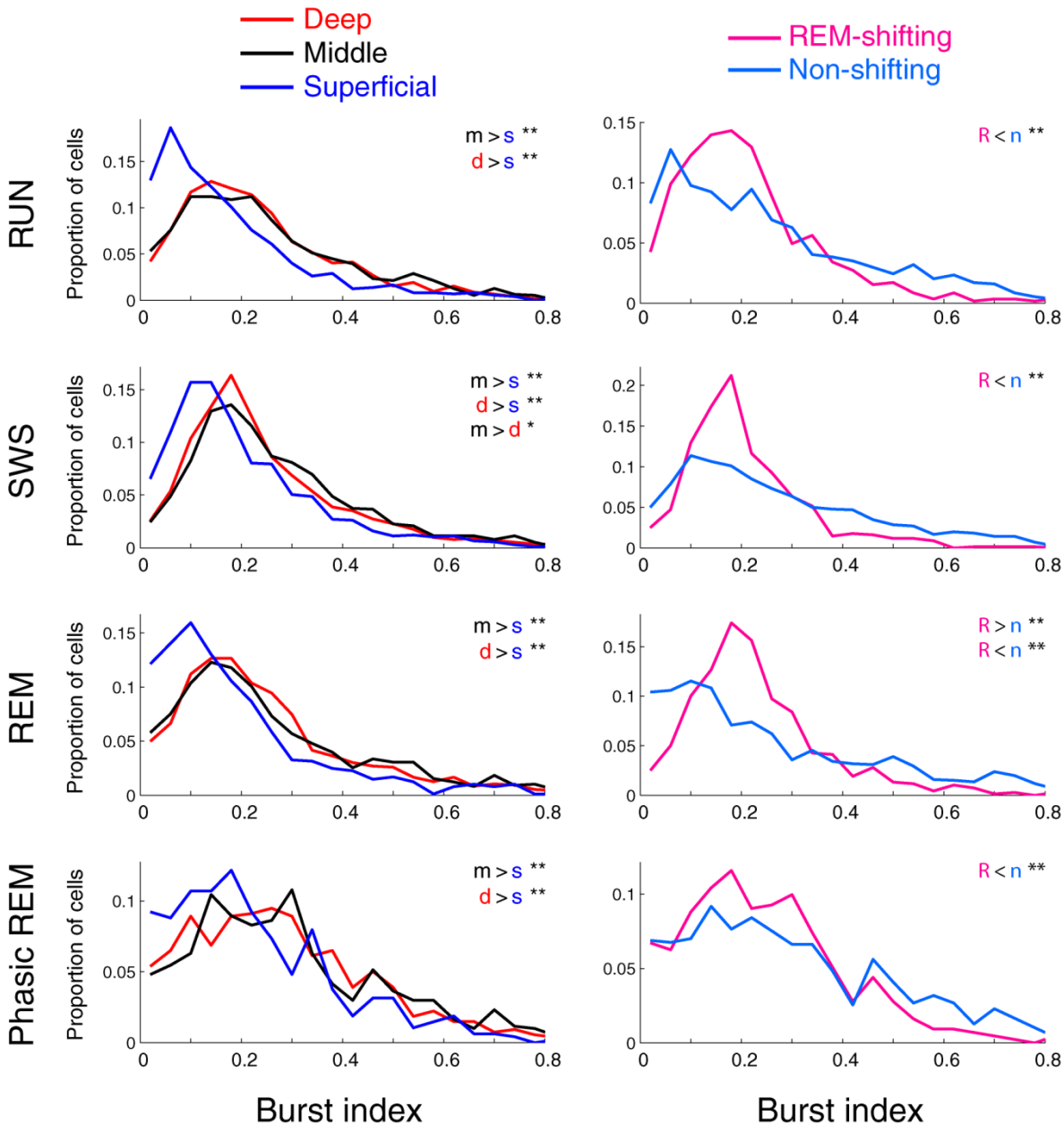

Supplementary Fig. 6. Burst index of CA1 pyramidal neurons depends on both the network state and the somatic location within the CA1 pyramidal layer. Distribution of burst index in different states, shown separately for deep, middle and superficial group (left) or REM-shifting and non-shifting neurons (right). **, $P < 0.0001$, *, $P < 0.01$, two-sample Kolmogorov-Smirnov test, one-tailed.

Figure S7

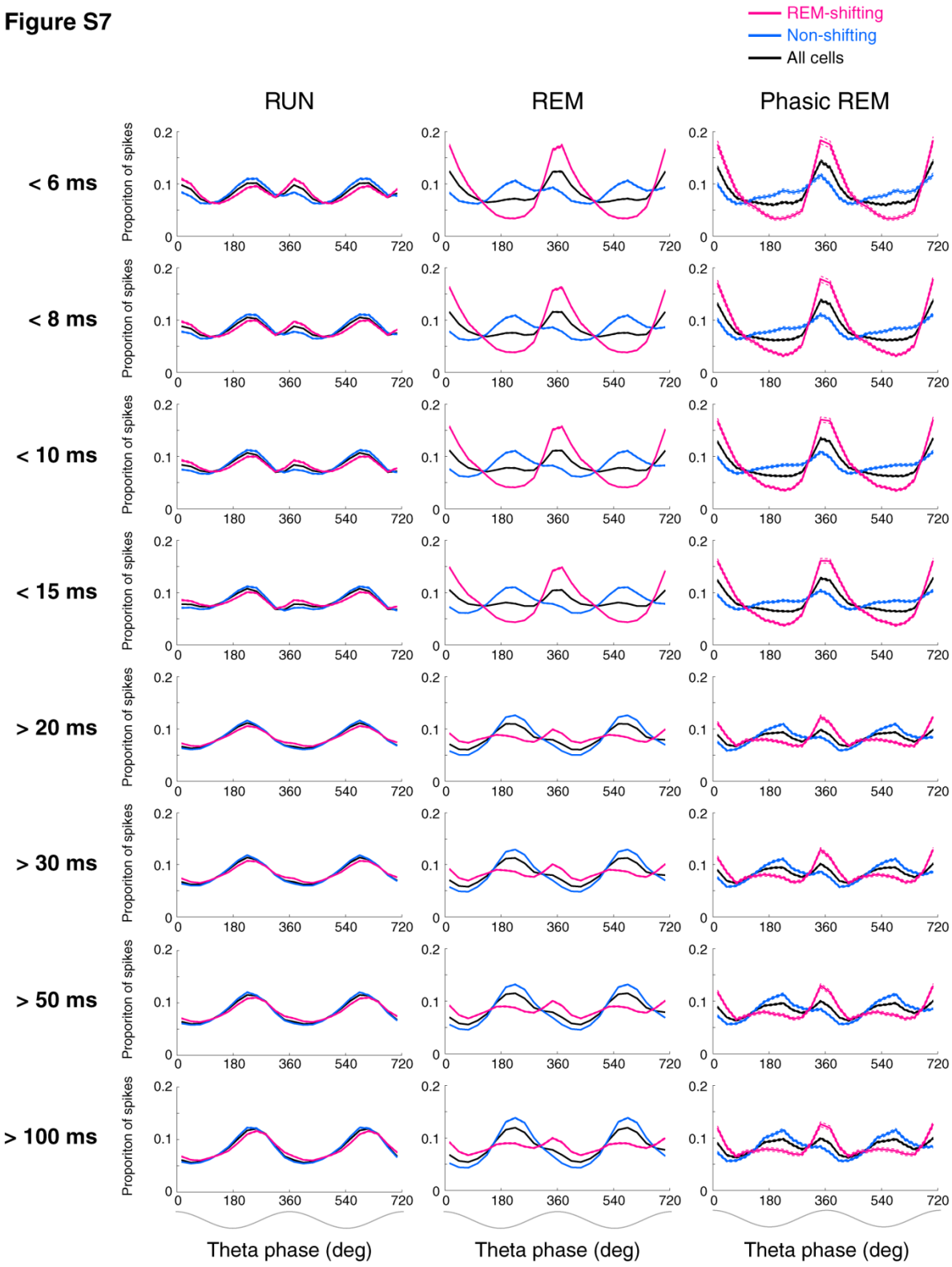
REM-shifting
Non-shifting
All cells
RUN
REM
Phasic REM
< 6 ms
< 8 ms
< 10 ms
< 15 ms
> 20 ms
> 30 ms
> 50 ms
> 100 ms
Proporiton of spikes
0
0.1
0.2
0
180
360
540
720
Theta phase (deg)

Supplementary Fig. 7. State-dependent shifting of theta phase preference of bursts and single spikes. Normalized theta phase histograms of spikes from all CA1 pyramidal cells (black). RUN, REM and phasic REM sleep are shown separately. Eight insterspike interval ('rate') categories are shown separately. This figure is complementary to **Fig. 5**, in which the distributions of the preferred phases of only the significantly modulated neurons in each ISI category are shown. Note second peak of phase-locked activity at the peak of theta for burst spikes (< 15 msec) during RUN. Theta peak preference increased during REM and even more so during phasic REM epochs. The REM-shifting (see **Fig. 2**, magenta) and non-shifting groups (light blue) are also shown. Bursts of REM-shifting neurons occurred almost exclusively at the theta peak during REM and phasic REM episodes. Theta phase histogram of each neuron for each ISI category was first normalized by the number of each neuron's spike for each ISI category. Mean ± S.E.M. for each neuron group is shown. Bottom gray traces, idealized reference theta cycle in CA1 pyramidal layer.

Figure S8

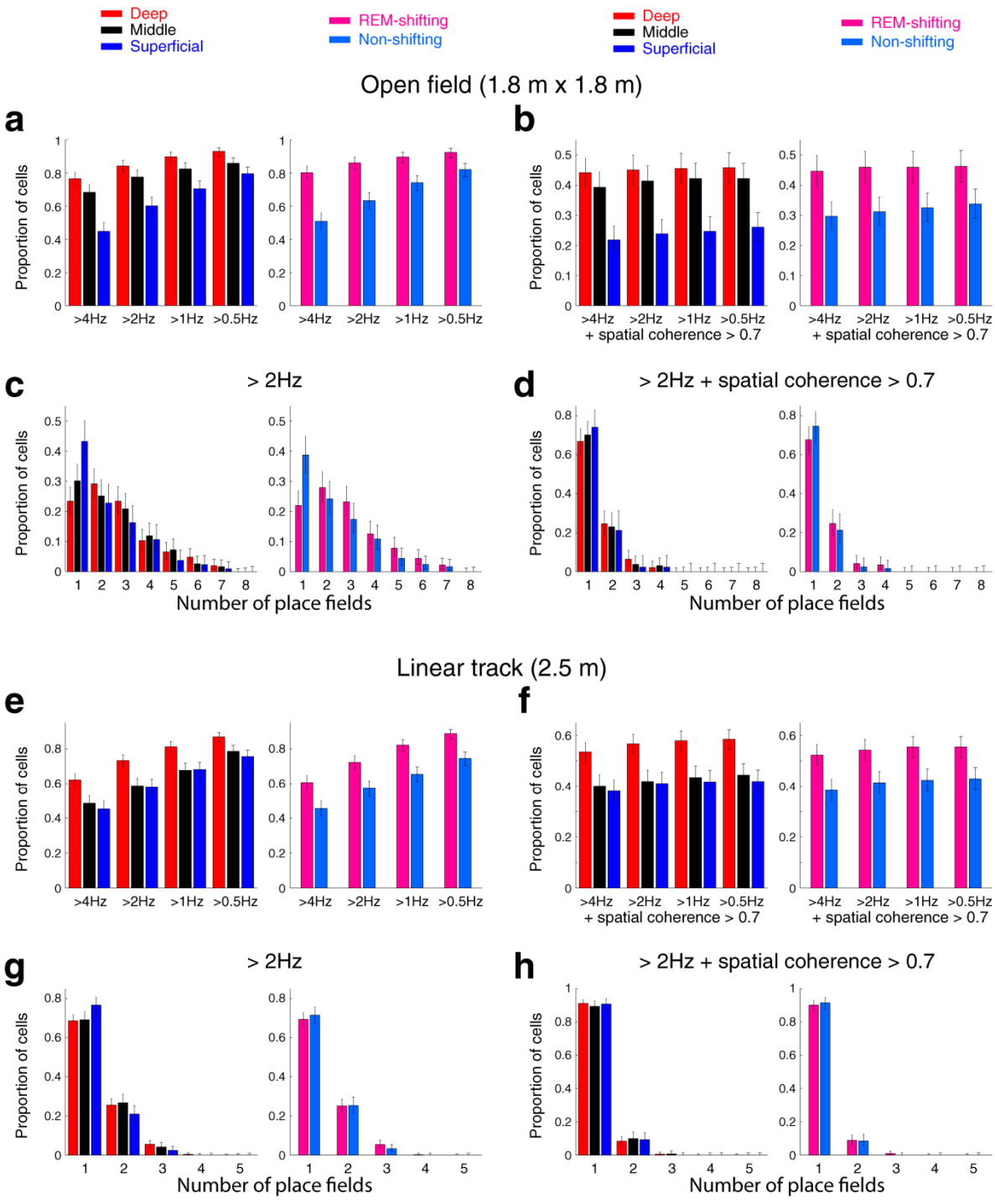
Deep
Middle
Superficial
REM-shifting
Non-shifting
Open field (1.8 m x 1.8 m)
a
b
Proportion of cells
>4Hz
>2Hz
>1Hz
>0.5Hz
+ spatial coherence > 0.7
c
> 2Hz
d
> 2Hz + spatial coherence > 0.7
Number of place fields
Linear track (2.5 m)
e
f
g
h

Supplementary Figure 8. Behavioral correlates of deep, middle and superficial CA1 pyramidal neurons, and REM-shifting and non-shifting cells. a-d. Data collected during open field exploration. **e-h.** Data collected during running on the linear track. **a.** Proportion of cells with place fields. The effect of depth within the CA1 pyramidal layer (left) and comparison between REM-shifting and non-shifting cells (right), as in **Fig. 6**. Here, four categories of place cells are shown, defined by their within-field peak firing rates. Clopper-Pearson confidence intervals ($P < 0.05$) are shown**. b**. Same displays as in a, but place fields were defined by the combination of peak firing rates and spatial coherence. Only fields with spatial coherence > 0.7 were regarded as place fields (for the definition of spatial coherence, see Online Methods). Note that regardless of the definition of place fields, the deep and REM-shifting groups had higher proportion of place cells than superficial and non-shifting groups, although the addition of the spatial coherence criterion reduced the number of eligible neurons substantially. **c**. Number of place fields per neuron, where place fields were defined by peak firing rate > 2 Hz. **d**. Number of place fields per neuron, where place fields were defined by peak firing rate > 2 Hz and spatial coherence > 0.7. Note that after adding the spatial coherence criterion, sublayer differences and differences between REM-shifting and non-shifting neurons largely disappeared. Clopper-Pearson confidence intervals ($P < 0.05$) are shown. **e** to **h**. Same comparisons for the linear track. For the linear track, pyramidal cells which had place fields at least in one direction were defined as place cells. Number of place fields was determined in each direction separately.

Figure S9

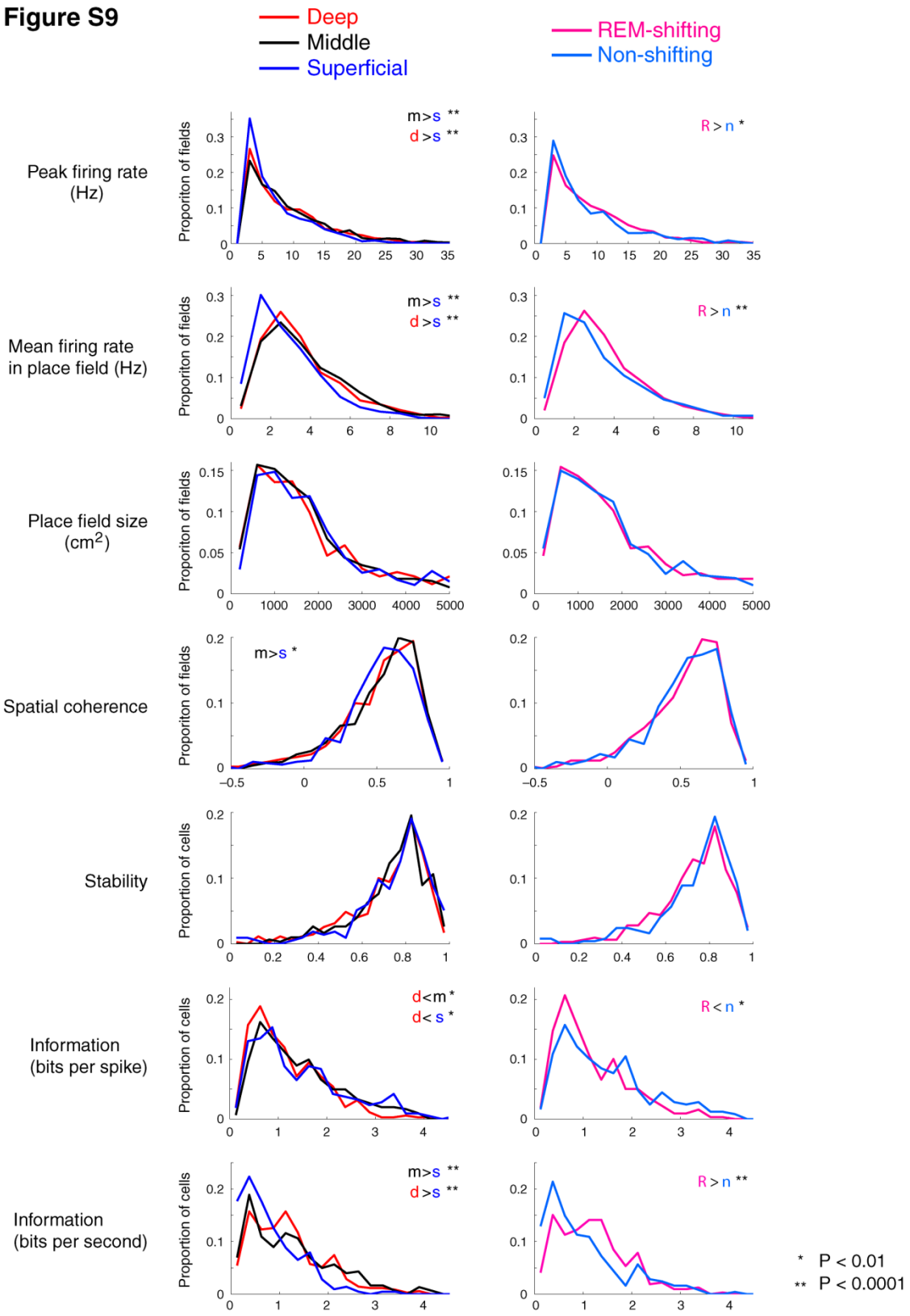
Deep
Middle
Superficial
REM-shifting
Non-shifting
Peak firing rate (Hz)
Mean firing rate in place field (Hz)
Place field size (cm2)
Spatial coherence
Stability
Information (bits per spike)
Information (bits per second)
Proportion of fields
Proportion of cells
m>s **
d>s **
R>n *
R>n **
m>s *
d<m *
d< s *
R<n *
* P < 0.01
** P < 0.0001

Supplementary Figure 9. Behavioral correlates of deep, middle and superficial CA1 pyramidal neurons (left columns), and REM-shifting and non-shifting cells (right columns). All data are from open field exploration. Place fields were defined by firing rate (> 2Hz) criterion alone. For the definition of spatial measures, consult Online Methods. P-value; two-sample Kolmogorov-Smirnov test, one-tailed.

Information content per spike was higher in the superficial and non-shifting groups than in the deep and REM-shifting groups. An opposite relation was present for information content per second. These discrepancies can be accounted for by the higher firing rates of deep and REM-shifting groups.

Figure S10

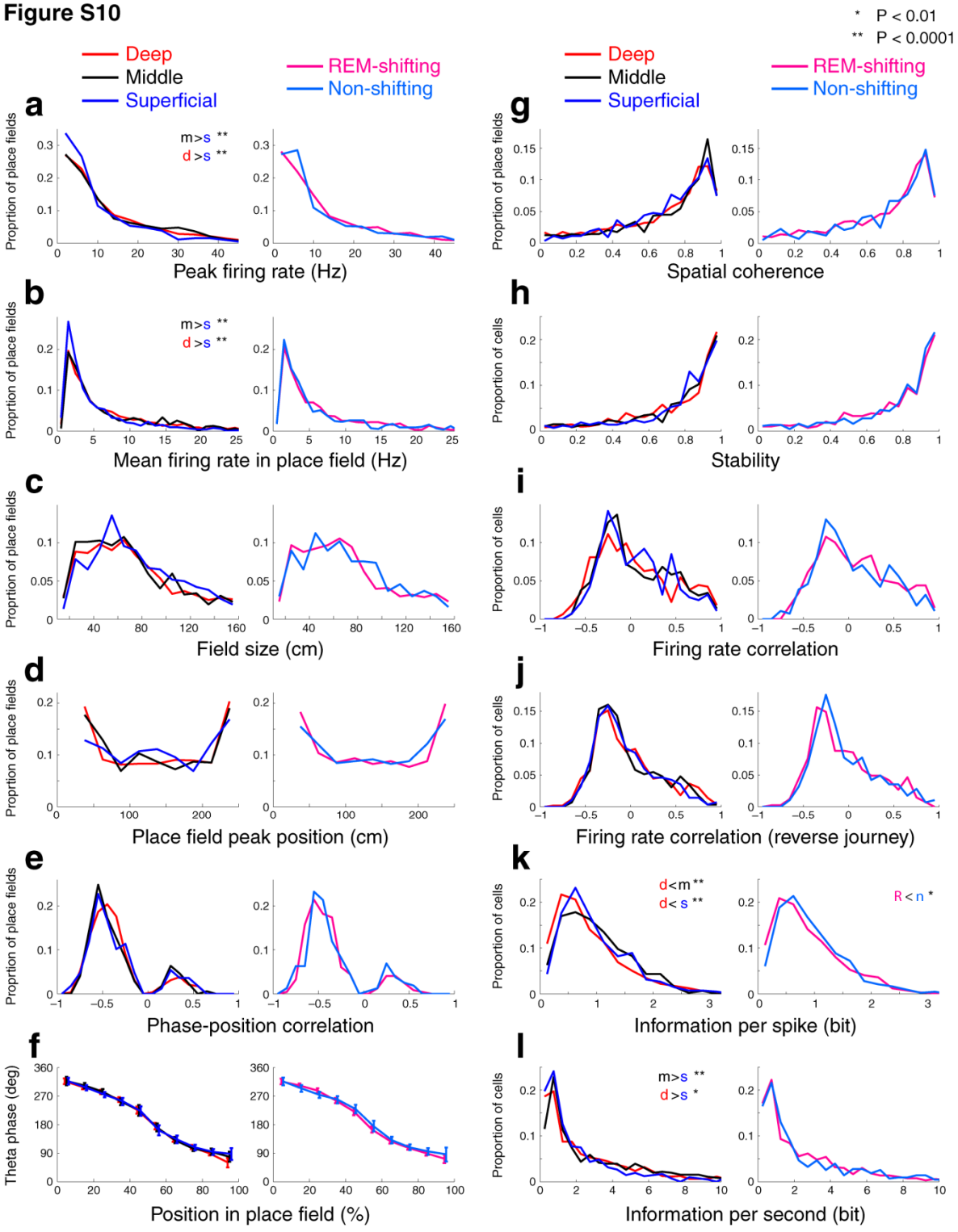
* P < 0.01
** P < 0.0001
Deep
Middle
Superficial
REM-shifting
Non-shifting
a
m>s **
d >s **
Proprtion of place fields
Peak firing rate (Hz)
b
Mean firing rate in place field (Hz)
c
Field size (cm)
d
Place field peak position (cm)
e
Phase-position correlation
f
Theta phase (deg)
Position in place field (%)
g
Spatial coherence
h
Proportion of cells
Stability
i
Firing rate correlation
j
Firing rate correlation (reverse journey)
k
d<m **
d< s **
R < n *
Information per spike (bit)
l
m>s **
d >s *
Information per second (bit)

Supplementary Figure 10. Behavioral correlates of deep, middle and superficial CA1 pyramidal neurons (left columns), and REM-shifting and non-shifting cells (right columns). All data were collected during linear track running. Place fields were defined by firing rate (> 2Hz) criterion alone. Distribution of peak firing rate (**a**) or mean rate within fields (**b**). Note that the significant differences were present only for neurons with < 5 Hz rates. **d.** Distribution of place field peak position. 0 cm = start position, 250 cm = rewarded end. Area at 0-25cm was excluded from the analysis to exclude the effect of behavioral variability. **f**. Mean phase precession slopes were not different in any comparison. For the definition of other spatial measures, consult Online and Supplementary Methods. P-value; two-sample Kolmogorov-Smirnov test, one-tailed.

Information content per spike was higher in the superficial than in the deep group. An opposite relation was present for information content per second. This discrepancy can be accounted for by the higher firing rates of deep group.

Figure S11

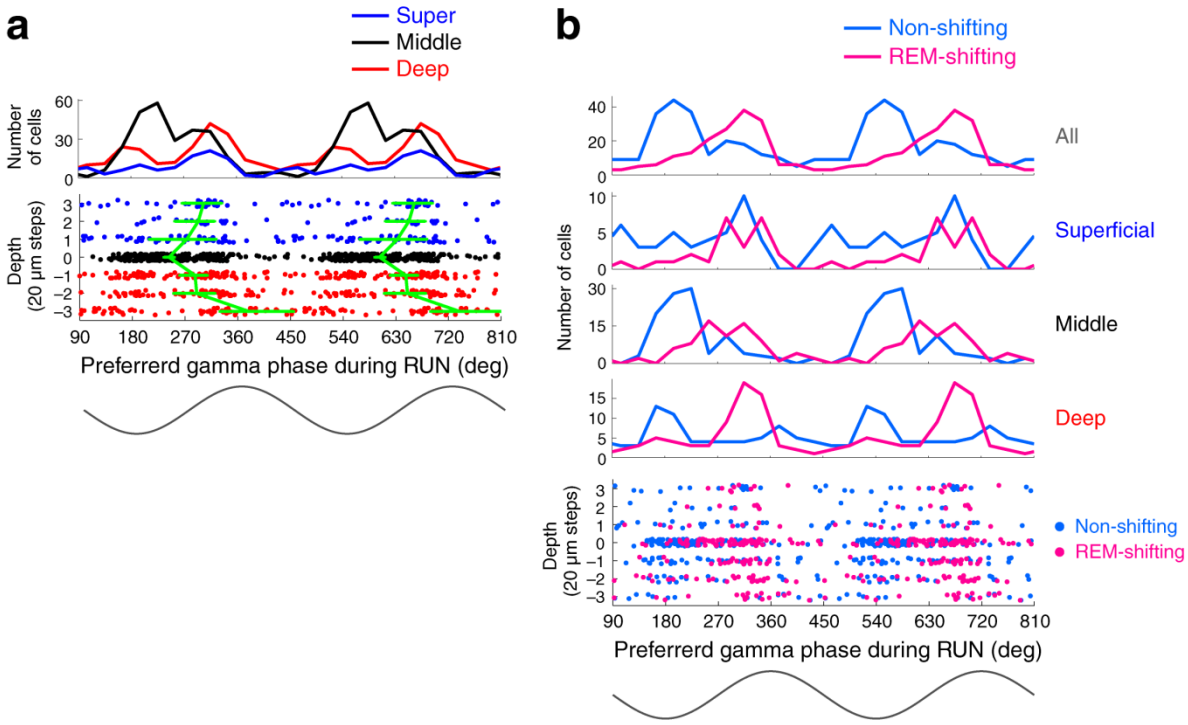

Supplementary Figure 11. Preferred gamma phase during RUN as a function of depth in the CA1 pyramidal layer. a. Top, distribution of the preferred gamma phase of pyramidal cells in the superficial (blue), middle (black) and deep (red) sublayers during RUN. Bottom, each dot represents a single neuron. The few neurons above and below recording sites 3 and –3 were added to values at 3 and –3, respectively. Position 0, approximate middle of the layer (black dots) was determined by the maximum of ripple power for each shank in each session (see **Fig. 1**). Green lines, mean (± 95% confidence intervals) of preferred gamma phase of pyramidal cells during RUN at different depths of the layer. **b,** Distribution of gamma phase preference during maze running (RUN), shown separately for REM-shifting and non-shifting neurons in all and separate sublayers. Note separation of preferred gamma phase of REM-shifting and non-shifting neurons in the middle and deep sublayers. Bottom, depth distribution of gamma phase preference of individual REM-shifting and non-shifting neurons.

Figure S12

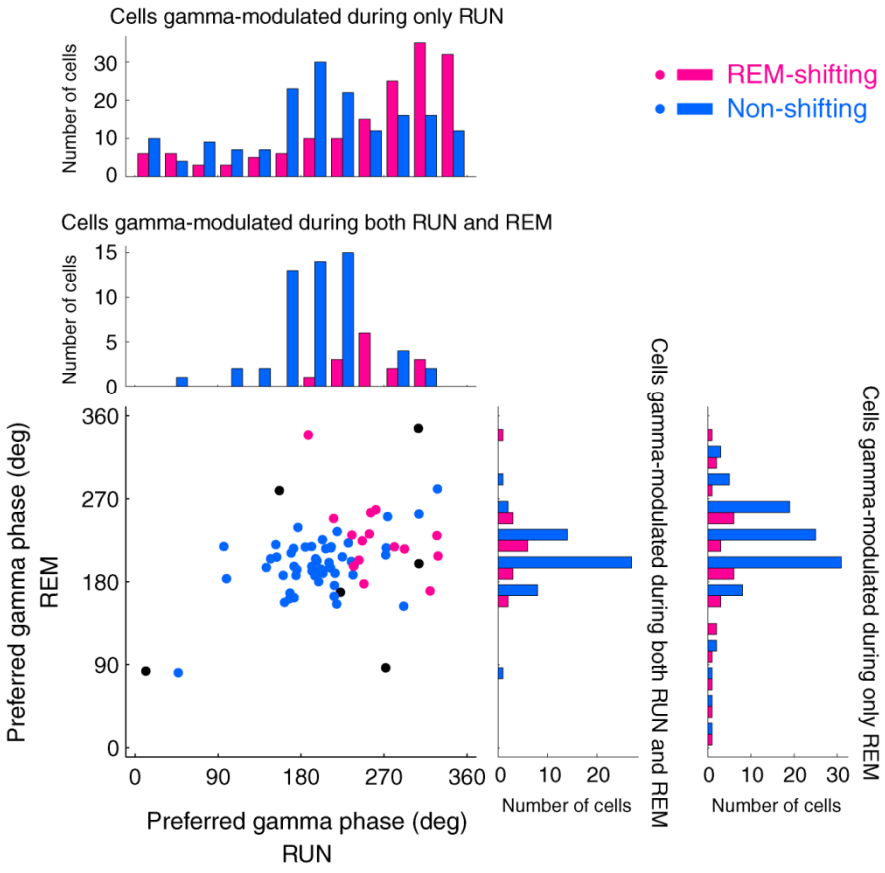

Supplementary Figure 12. State-dependence of gamma phase coupling of CA1 pyramidal cells. Distribution of gamma phase preference during RUN (top histogram, significantly gamma modulated during only RUN) and for a subgroup of neurons, which were significantly phase-locked to gamma oscillations during both RUN and REM sleep (second histogram). REM-shifting and non-shifting neurons are shown separately. Note that very few pyramidal cells were phase-locked to gamma during both RUN and REM states. The scatter plot shows the preferred gamma phase of the same neurons during RUN and REM. Only neurons significantly gamma-modulated in both states are shown. Black dots, neurons not significantly theta-modulated during REM sleep. Note that the preferred phase shifted from the rising phase during RUN to the trough of gamma during REM. Right-most histogram, distribution of neurons, which were significantly phase-locked to gamma only during REM. Note similar gamma phase preference of REM-shifting and non-shifting cells during REM.

Figure S13

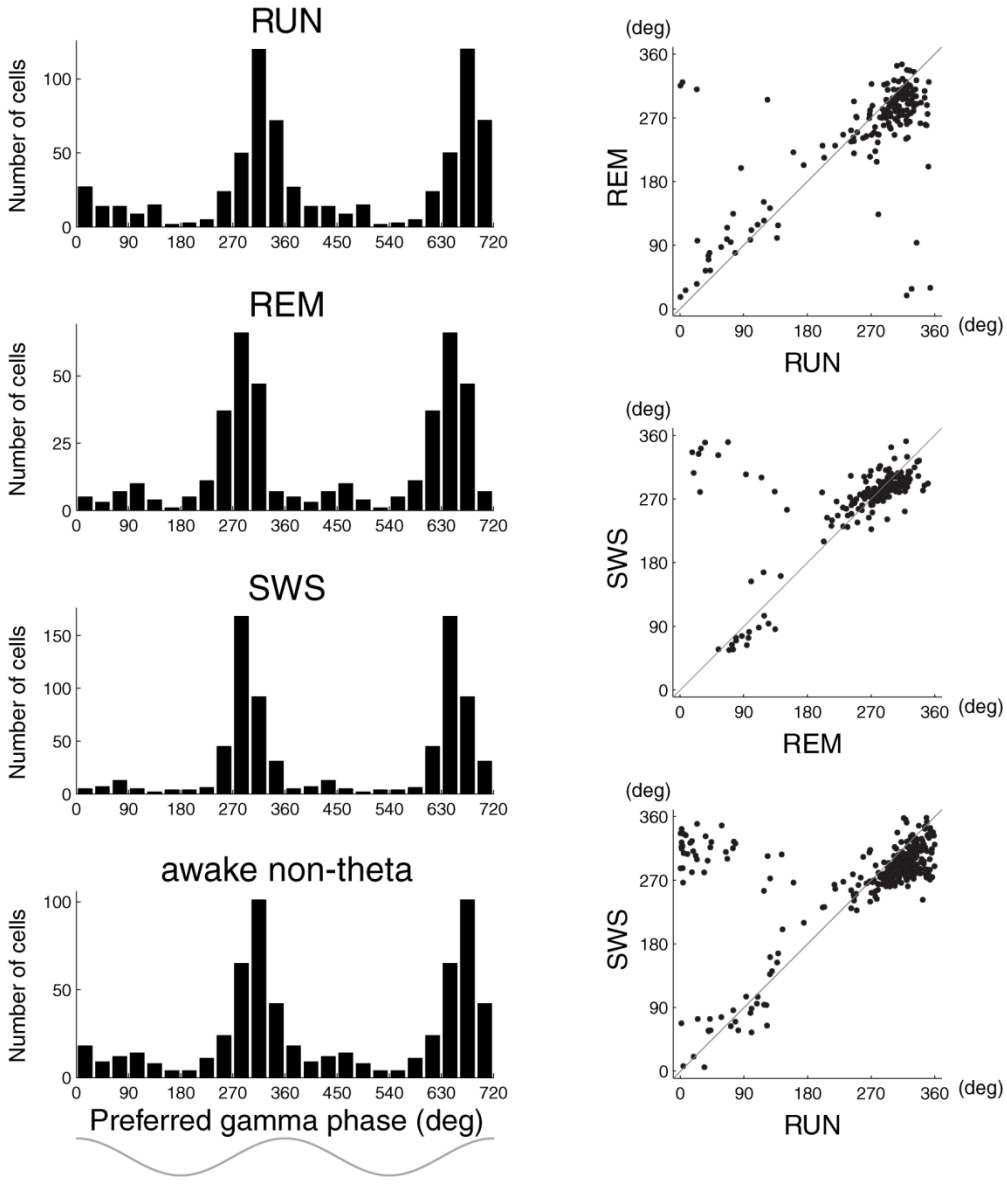

Supplementary Fig. 13. Phase preference of CA1 interneurons is stable across states. Left, Distribution of gamma phase preference of putative CA1 interneurons during RUN, REM, slow wave sleep (SWS) and during awake non-theta in the absence of theta oscillations. Right, comparison of preferred gamma phase preference across states. Only neurons with significant gamma phase modulation in the corresponding two states are included. Note gamma phase stability of interneurons across various states. Bottom gray trace, idealized reference gamma cycle in CA1 pyramidal layer.

Figure S14

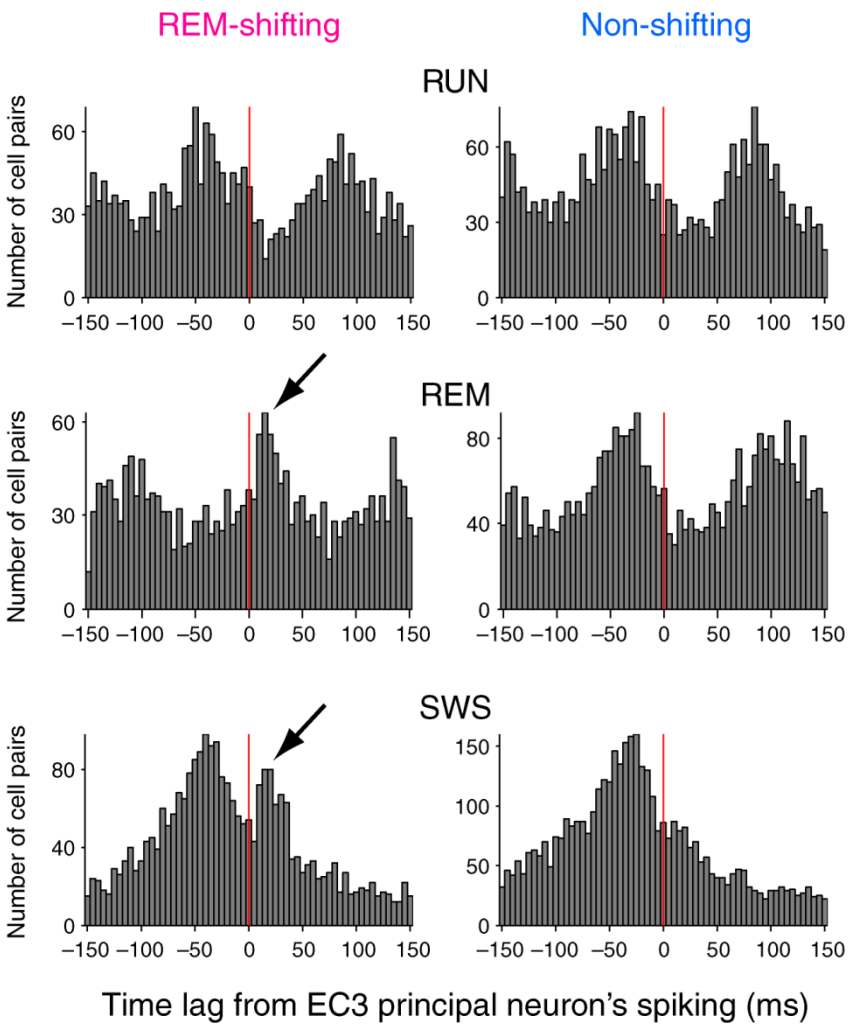

Supplementary Fig. 14. State-dependent relationship between entorhinal layer 3 (EC3) and CA1 pyramidal cells. Distribution of cross-correlation peaks between spikes of EC3 principal neurons and CA1 neurons, shown separately for REM-shifting and non-shifting neurons during RUN, REM and SWS. Note that during RUN, activity of CA1 neurons peaked ~ 80 msec after the spike of the reference EC3 neurons[2] (time zero). In contrast, during REM, a fraction of REM-shifting neurons fired much earlier (arrow), whereas non-shifting neurons kept the same temporal relationship with EC3 neurons as during RUN. During SWS, a fraction of REM-shifting neurons fired 10-30 msec after EC3 neurons (arrow). The peak firing of CA1 pyramidal cells prior to the reference EC3 spike during SWS may reflect CA1 ripple-burst activation of EC3 neurons[2]. Note that these spike-spike cross-correlation data during RUN and REM are similar to those shown in **Supplementary Fig. 3**, where neuronal discharges were referenced to theta phase.